

X-Ray Reflection Nebulae with Large Equivalent Widths of Neutral Iron $K\alpha$ Line in the Sgr C Region

Hiroshi NAKAJIMA

Department of Earth and Space Science, Graduate School of Science, Osaka University, Toyonaka, Osaka, 560-0043

nakajima@ess.sci.osaka-u.ac.jp

Takeshi Go TSURU, Masayoshi NOBUKAWA, Hironori MATSUMOTO,

and

Katsuji KOYAMA

Department of Physics, Graduate School of Science, Kyoto University, Sakyo-ku, Kyoto, 606-8502

Hiroshi MURAKAMI

Department of Physics, Rikkyo University, 3-34-1, Nishi-Ikebukuro, Toshima-ku, Tokyo, 171-8501

Atsushi SENDA

RIKEN (The Institute of Physical and Chemical Research), 2-1, Hirosawa, Wako, Saitama, 351-0198

and

Shigeo YAMAUCHI

Faculty of Humanities and Social Sciences, Iwate University, 3-18-34, Ueda, Morioka, Iwate, 020-8550

(Received 0 0; accepted 0 0)

Abstract

This paper reports on the first results of the Suzaku observation in the Sgr C region. We detected four diffuse clumps with strong line emission at 6.4 keV, $K\alpha$ from neutral or low-ionized Fe. One of them, M 359.38–0.00, is newly discovered with Suzaku. The X-ray spectra of the two bright clumps, M 359.43–0.07 and M 359.47–0.15, after subtracting the Galactic center diffuse X-ray emission (GCDX), exhibit strong $K\alpha$ line from FeI with large equivalent widths (EWs) of 2.0–2.2 keV and clear $K\beta$ of FeI. The GCDX in the Sgr C region is composed of the 6.4 keV- and 6.7 keV-associated components. These are phenomenologically decomposed by taking relations between EWs of the 6.4 keV and 6.7 keV lines. Then the former EWs against the associated continuum in the bright clump regions are estimated to be $2.4_{-0.7}^{+2.3}$ keV. Since the two different approaches give similar large EWs of 2 keV, we strongly suggest that the 6.4 keV clumps in the Sgr C region are due to X-ray reflection/fluorescence (the X-ray reflection nebulae).

Key words: Galaxy: center — ISM: clouds — ISM: molecules — X-rays: ISM

1. Introduction

The Galactic center (GC), the nearest galactic nucleus, hosts various classes of high energy sources such as super massive black hole Sgr A*, X-ray binaries, supernova remnants, and non-thermal filaments (NTFs). GC is also the primary site of giant molecular clouds (MCs) and star formation inside the MCs. One of the most interesting characteristics in GC is the diffuse 6.4 keV emission from neutral iron (FeI). Most of the prominent 6.4 keV emissions are found in the MCs of Sgr B2 (Koyama et al. 1996), G 0.13–0.13 (Yusef-Zadeh et al. 2002), Sgr B1 (Nobukawa et al. 2008), and Sgr C (Murakami et al. 2001b). A number of small MCs in the GC region also emit strong 6.4 keV line (Predehl et al. 2003; Park et al. 2004).

For the origin of 6.4 keV emission line from MCs, two models have been proposed. One is the impact of low-energy cosmic-ray electrons (LECRE) followed by bremsstrahlung and 6.4 keV line emission, proposed for the origin of the Galactic Ridge X-ray Emission (Valinia et al. 2000). Yusef-Zadeh et al. (2002) proved that this model can be applied to G 0.13–0.13 assuming the Fe abundance of two solar. The other is that the hard X-rays and 6.4 keV lines are due to reflection/fluorescence from MCs irradiated by external hard X-ray sources (X-ray reflection Nebulae; XRNe) (Sunyaev et al. 1993; Markevitch et al. 1993; Koyama et al. 1996; Sunyaev & Churazov 1998; Park et al. 2004). Since no irradiating source capable of powering the 6.4 keV line was found, Koyama et al. (1996) proposed a scenario of a past X-ray outburst of the super massive black hole at Sgr A*. The present luminosity is $2 \times 10^{33} \text{erg s}^{-1}$ (Baganoff et al. 2001; Baganoff et al. 2003), and hence it would have been 10^6 times brighter than now 300 years ago.

In fact, the Chandra observation shows that the 6.4 keV emission line of the giant MC Sgr B2 has a concave shape pointing to the GC direction (Murakami et al. 2001a). The broad band spectrum of Sgr B2 is well described by Compton scattered and reprocessed radiation emitted in the past by Sgr A* (Revnivtsev et al. 2004). The morphology and flux of the 6.40 keV line of Sgr B2 have been time variable for 10 years (Muno et al. 2007; Koyama et al. 2008a; Inui et al. 2008). Thus observational results supporting the XRNe rather than the LECRe model have been accumulating for Sgr B2. However, for the other regions, in particular Sgr C, observations have been limited and hence the 6.4 keV line origin is still open issue.

The Sgr C region consists of giant MCs and large H II regions. From the ^{13}CO observations, Liszt & Spiker (1995) estimated 6.1×10^5 solar mass for the molecular gas. Murakami et al. (2001b) discovered a 6.4 keV clump with ASCA, and interpreted that the clump is an XRNe because the X-ray spectrum exhibited a large equivalent width (EW) of the 6.4 keV emission line with a strong absorption like that in Sgr B2. On the other hand, Yusef-Zadeh et al. (2007) discussed possible association of the 6.4 keV emission lines with some radio NTFs based on the Chandra observation, and argued that the 6.4 keV line is due to the impact of LECRe. These results and arguments are based on the short exposure observations (20 ksec and 22 ksec for

the ASCA and Chandra, respectively). In order to fix the above debates, we, therefore, made a long Suzaku observation on the Sgr C region.

For simplicity, we use “the east” as the positive Galactic longitude side, and “the north” as the positive Galactic latitude side. We assume the distance to the Sgr C region to be 8.5 kpc following the recommendation of IAU. We applied the solar abundance and photoelectric absorption cross-section from the tables given by Anders & Grevesse (1989) and Balucinska-Church & McCammon (1992), respectively.

2. Observation and Data Reduction

The Sgr C region was observed with the XIS (X-ray Imaging Spectrometer) from 2006 Feb. 20 to 23. The telescope optical axis position was R.A.=17^h44^m37^s.30, Decl.= −29°28′10″.2 (J2000.0). The XIS consists of four sets of the X-ray CCD camera systems placed on the focal planes of the four X-Ray Telescopes (XRT) onboard the Suzaku satellite. One of the XIS sensors (XIS1) has a back-illuminated (BI) CCD, while the other three sensors (XIS0, 2 and 3) utilize front-illuminated (FI) CCDs. The detailed descriptions of the Suzaku satellite, XRT, and XIS can be found in Mitsuda et al. (2007), Serlemitsos et al. (2007), and Koyama et al. (2007a), respectively.

A cleaned event list was obtained from the processed data with the version of 2.0.6.13¹ by removing events taken during the passage of the South Atlantic Anomaly, the elevation angles from the night Earth rim of < 5° and from the sun-lit Earth rim of < 20°, and the telemetry saturation. After these data screenings, the net exposure was 107 ksec. We analyzed the screened data using the HEADAS software version 6.4, XSPEC version 11.3.2g². We utilized the calibration databases released on 2008 Feb. 1³.

3. Analysis and Results

The non X-ray (particle) background (NXB) becomes serious in the hard X-ray band, in particular for diffuse sources. The flux of the NXB is correlated with the geomagnetic cut-off rigidity (COR) (Tawa et al. 2008). We, therefore, made COR-sorted NXB data sets using the night-Earth data released by the Suzaku XIS team⁴. For the following imaging and spectral studies in the Sgr C region (section 3.1 and 3.2), we used the X-ray data after subtracting the NXB that were compiled to have the same COR distribution as that during the Sgr C observation.

To increase statistics, here and after, we co-added the four XIS data for imaging study,

¹ <http://www.astro.isas.jaxa.jp/suzaku/process/>

² <http://heasarc.gsfc.nasa.gov/docs/software/lheasoft/>

³ <http://www.astro.isas.jaxa.jp/suzaku/caldb/>

⁴ <http://www.astro.isas.jaxa.jp/suzaku/analysis/xis/nxe/>

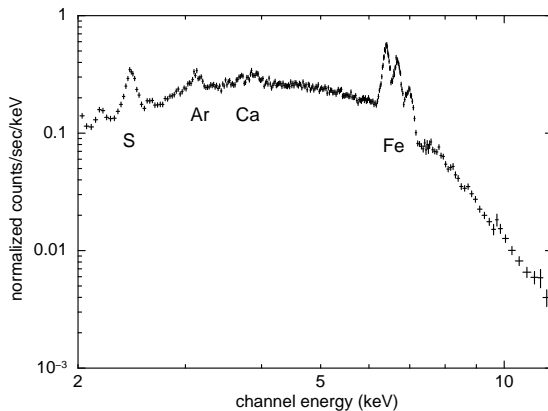


Fig. 1. The co-added GCDX spectrum of the FIs (XIS0+2+3) in the Sgr C region extracted from the 6'95 radius circle in the center of the XIS FOV. The NXB component was subtracted. The spectrum of BI (XIS1) was simultaneously analyzed, but the figure is not shown here, for brevity.

in which exposure and vignetting correction were made. For the spectral study, we co-added the three FI CCD data, and treated BI data separately because the response functions are significantly different between FI and BI.

3.1. X-ray Image in the Emission Line

Figure 1 shows the energy spectrum of the whole Sgr C region, which was extracted from the circular region with a radius of 6'95 from the FOV center. The spectrum shows K-shell emission lines from He-like and/or H-like ions of S, Ar, Ca, and Fe. In addition, the 6.4 keV emission line and the K-edge absorption at 7.1 keV due to FeI are detected. The three Fe K-shell emission lines at 6.4, 6.7 and 6.9 keV in the Galactic center diffuse X-ray emission (GCDX)(Koyama et al. 1989; Yamauchi et al. 1990; Koyama et al. 2007b) are clearly resolved.

Since the Suzaku coordinate has 90% confident error of 19'' (Uchiyama et al. 2008), we made coordinate correction using a Chandra observation. In the energy band of 0.7–1.5 keV, a point source with the flux of $\sim 6 \times 10^{-15}$ erg cm $^{-2}$ s $^{-1}$ was detected at (R.A., Decl.) $_{J2000.0}=(17^{\text{h}}44^{\text{m}}52^{\text{s}}.1, -29^{\circ}31'56''.7)$ in the XIS image. In the error circle of Suzaku, there was only one Chandra point source at (R.A., Decl.) $_{J2000.0}=(17^{\text{h}}44^{\text{m}}53^{\text{s}}.1, -29^{\circ}31'45''.5)$. Since the flux was almost the same as that of the Suzaku source, we safely concluded these point sources are identical. We, then fine-tuned the Suzaku coordinate by shifting $\Delta(\text{R. A., Decl.})=(13''.7, 11''.2)$.

Referring figure 1, we made the narrow band image of the 2.45 keV-line (2.35–2.50 keV; $K\alpha$ of SXV) and the 6.4 keV-line (6.28–6.42 keV; $K\alpha$ of FeI). The images after the smoothing with the Gaussian kernel of 48 pixels (0'83) are shown in figure 2. In figure 2(a), a bright 2.45 keV-line clump is found at $(l, b) = (359^{\circ}407, -0^{\circ}119)$, hence designated as G 359.41–0.12. Likely, four 6.4 keV-line clumps found in figure 2(b) are designated as M 359.43–0.07, M 359.47–0.15, M 359.43–0.12, and M 359.38–0.00, where M 359.43–0.12 is

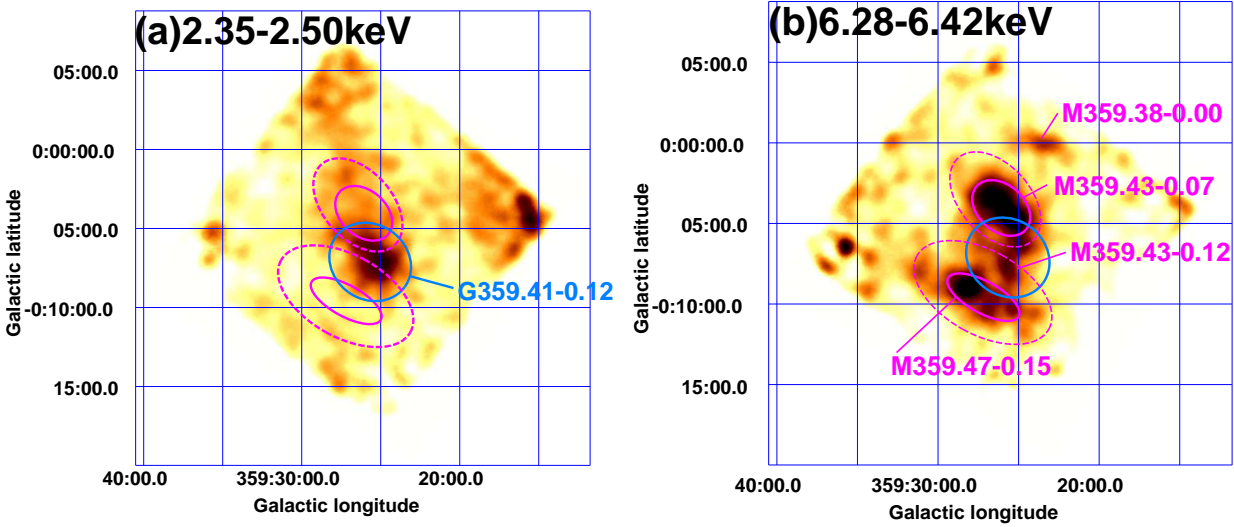


Fig. 2. (a) The 2.45 keV-line ($K\alpha$ -S XV) image in the energy band of 2.35–2.50 keV and (b) the 6.4 keV-line ($K\alpha$ of Fe I) image in the 6.28–6.42 keV band. The source and background regions for the spectral analysis are shown with the solid and dashed magenta ellipses, where the data within the blue ellipse (G 359.41–0.12) were excluded to minimize the contamination from the strong 2.45 keV emission line and its associated continuum.

in the region of G 359.41–0.12.

3.2. The Emission Line Feature in the Sgr C Region

The photon statistics are limited to make measurable spectra for M 359.38–0.00 and M 359.43–0.12. Furthermore, M 359.43–0.12 is in the 2.45 keV-source, G 359.41–0.12. Therefore we concentrated on the two bright sources, M 359.43–0.07 and M 359.47–0.15, and the surrounding background regions.

As is seen in figure 1, the GCDX with strong 6.7 keV ($K\alpha$ of Fe XXV) and 6.9 keV ($Ly\alpha$ of Fe XXVI) lines is the largest background for the local enhancements such as the 6.4 keV-clumps. In addition, the flux of the GCDX is not uniform but variable from position to position. To see the flux distribution and nature of the GCDX near Sgr C, we examined the NXB-subtracted (GCDX is not subtracted) spectra in the 6.4-keV clumps and the surrounding areas including candidate background regions (see figure 2).

The spectra from the whole Sgr C region is already made in section 3.1 (figure 1). The spectra of M 359.43–0.07 and M 359.47–0.15 are extracted from the regions shown with the solid magenta ellipses in figure 2(b). The background spectra for these 6.4 keV clumps were obtained from the annuli between the inner solid and outer dashed ellipses. Since G 359.41–0.12, the solid blue ellipse in figure 2(a), may have strong 2.45 keV-line with an associated continuum emission, we excluded G 359.41–0.12 from the spectra of the 6.4-keV sources and their backgrounds. As the surrounding area, we made additional spectrum from a circle at the

FOV center with a radius of 7.8 but excluding the above cited source and background regions (hereafter, the outer region).

The spectral fittings were made in the same energy band with the same phenomenological model and free parameters as those used in Koyama et al. (2007b, 2008b): a single power-law and 10 Gaussian emission lines. The spectra of FIs and BI were simultaneously fitted, and acceptable χ^2 were obtained from all the spectra. The FI spectra and the best-fit model of M 359.43–0.07 and M 359.47–0.15, and the outer region of Sgr C are shown in figure 3 as examples. The best-fit parameters are listed in table 1.

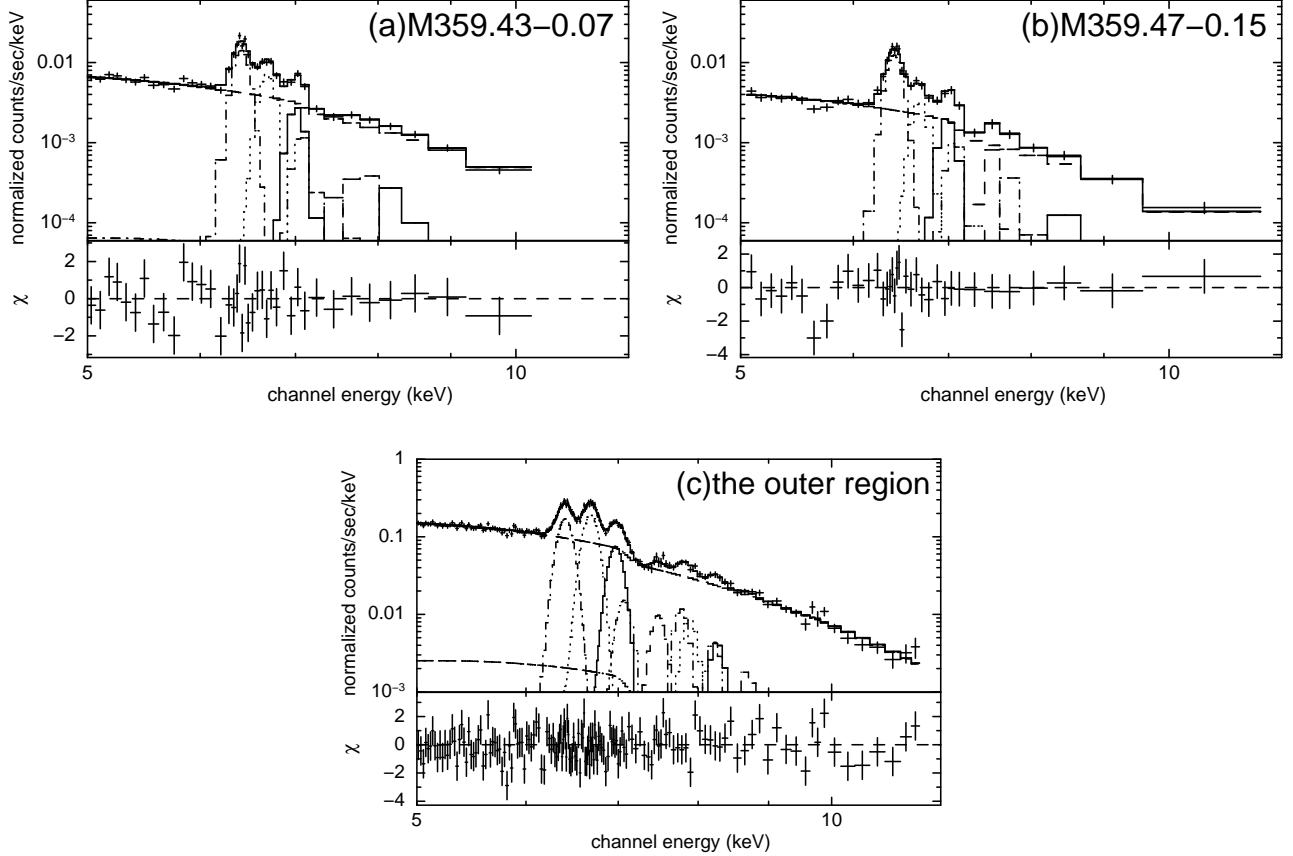


Fig. 3. Same as figure 1, but for M 359.43–0.07 (a), M 359.47–0.15 (b), and the outer region (c). The phenomenological model with single power-law, 10 Gaussian lines, and the cosmic X-ray background component is applied.

Koyama et al. (2008b) found that the GCDX in the Sgr A region is phenomenologically decomposed into the 6.7-keV line plus associated continuum (6.7-component) and the 6.4-keV line plus associated continuum (6.4-component); the EWs of the 6.4 keV ($EW_{6.4}$) and the 6.7 keV ($EW_{6.7}$) lines are given by the relation $EW_{6.7} + 0.50(\pm 0.06) \times EW_{6.4} = 0.62(\pm 0.07)$ [keV]. Then, in the limit of $EW_{6.4} \rightarrow 0$, $EW_{6.7}$ was estimated to be 0.62 ± 0.07 keV. On the other hand, in the limit of $EW_{6.7} \rightarrow 0$, $EW_{6.4}$ is 1.2 ± 0.2 keV. They also made the GCDX-subtracted spectra of the two 6.4 keV clumps in the Sgr A region (source 1 and 2 in Koyama et al. 2008b)

Table 1. The best-fit parameters for the NXB subtracted spectra.

Region	Area (arcmin ²)	Γ	Line Flux*		Line Equivalent width (eV)	
			$F_{6.4}$	$F_{6.7}$	$EW_{6.4}$	$EW_{6.7}$
(1)	152	1.72(1.65 – 1.78)	0.79(0.77 – 0.81)	0.68(0.65 – 0.70)	458(448 – 470)	420(401 – 430)
(2)	121	1.70(1.63 – 1.82)	0.55(0.53 – 0.57)	0.68(0.66 – 0.71)	346(333 – 363)	454(441 – 471)
(3)	7.09	1.82(1.65 – 2.06)	1.91(1.79 – 2.06)	1.08(0.96 – 1.22)	670(625 – 720)	400(357 – 454)
(4)	11.7	1.64(1.47 – 1.93)	1.00(0.92 – 1.08)	0.93(0.86 – 1.03)	397(365 – 428)	388(360 – 431)
(5)	6.91	1.96(1.59 – 2.24)	2.16(2.03 – 2.31)	0.63(0.53 – 0.73)	966(909 – 1030)	298(253 – 348)
(6)	22.4	1.75(1.59 – 1.97)	1.02(0.97 – 1.08)	0.67(0.62 – 0.72)	587(554 – 620)	404(374 – 437)

(1) the whole Sgr C region, (2) the outer region, (3) M 359.43–0.07, (4) background region for M 359.43–0.07, (5) M 359.47–0.15, (6) background region for M 359.47–0.15.

90% confidence limits are in parentheses.

* Absorption-uncorrected line flux in the unit of $10^{-6}\text{ph cm}^{-2} \text{ s}^{-1} \text{ arcmin}^{-2}$.

and obtained consistent $EW_{6.4}$ values as those estimated from the phenomenological relation.

Stimulated by the successful approach of Koyama et al. (2008b), we used the same method to decompose the GCDX in the Sgr C region into the 6.4-component and 6.7-component. Using the data in table 1, we plot the $EW_{6.4}$ and $EW_{6.7}$ relation of the six regions (figure 4). The outer region, the whole Sgr C and the background region for M 359.43–0.07 follow to, but the M 359.43–0.07 and M 359.47–0.15 regions come above the best-fit correlation line of the Sgr A region; these are systematically larger $EW_{6.4}$ than the Sgr A region. The best-fit linear relations between $EW_{6.7}$ and $EW_{6.4}$ for all cited regions except the whole Sgr C is;

$$EW_{6.7} + 0.22(\pm 0.12) \times EW_{6.4} = 0.53(\pm 0.06)[\text{keV}], \quad (1)$$

where the errors mean 90% confidence levels.

This relation indicates that $EW_{6.7}$ in the 6.7-component is 0.53 ± 0.06 keV (at $EW_{6.4} \rightarrow 0$) for the Sgr C region, consistent with that of the Sgr A region of 0.62 ± 0.07 keV (Koyama et al. 2008b). On the other hand, $EW_{6.4}$ in the 6.4-component is $2.4_{-0.7}^{+2.3}$ keV (at $EW_{6.7} \rightarrow 0$), larger than those in the Sgr A region (Koyama et al. 2008b).

3.3. Spectra of M 359.43–0.07 and M 359.47–0.15

From table 1, we see that the 6.7 keV line flux in M 359.43–0.07 and M 359.47–0.15 are almost identical to those of the respective background regions. The 6.7 keV flux differences are 16% and 6% of those in M 359.43–0.07 and M 359.47–0.15, respectively. Since the 6.7 keV line flux is a good indicator of the flux of the GCDX (Koyama et al. 2007b, 2008b), we conclude that the background regions were properly selected within possible systematic error of 6–16%, which is smaller than the statistical errors.

Therefore we made the GCDX-subtracted spectra of these 6.4 keV clumps (figure 5). The energy-dependent vignetting were corrected by multiplying the effective-area ratio of the source region to corresponding background region for each energy bin of the GCDX spectra.

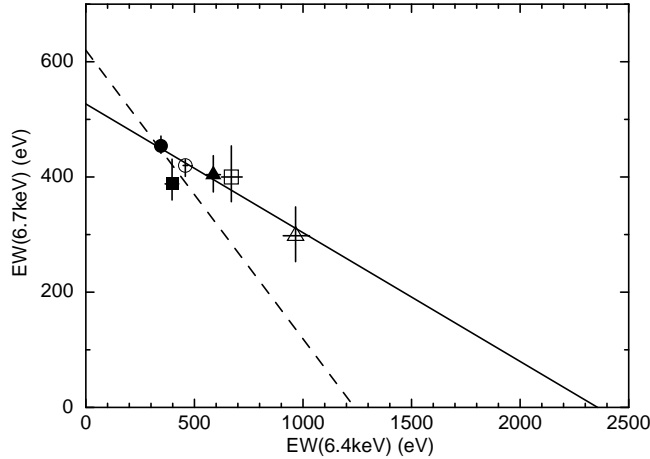


Fig. 4. The correlation between the EWs of the Fe I-K α line ($EW_{6.4}$) and Fe XXV-K α line ($EW_{6.7}$). The dashed line shows the best fit relation in the Sgr A region (adopted from figure 2(d) of Koyama et al. 2008b). The open and filled circle show the whole Sgr C region and the outer region, respectively. The source regions of M 359.43–0.07 and M 359.47–0.15 are plotted with the open square and triangle, while their background regions are given by the filled marks. The solid line is the best-fit relation for all regions except the whole Sgr C of $EW_{6.7} + 0.22 \times EW_{6.4} = 0.53[\text{keV}]$.

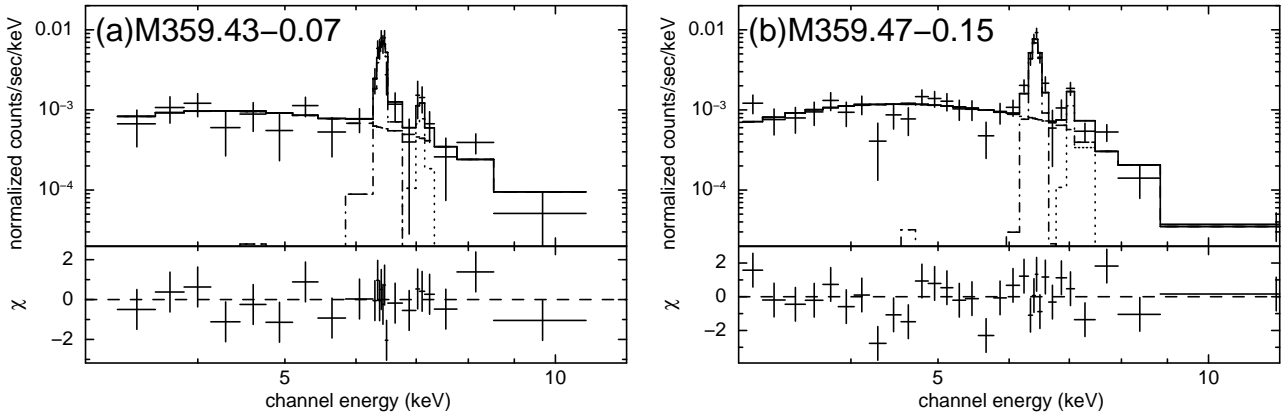


Fig. 5. Same as figure 3, but for GCDX-subtracted spectra of M 359.43–0.07 (a) and M 359.47–0.15 (b). The K α and K β emission lines of Fe I and power-law are shown by dot-dashed, dotted, and dashed lines, respectively.

We first applied a model of a power-law and a narrow Gaussian line at 6.4 keV with absorption. The metal abundances of the inter stellar medium were fixed to the solar value (Anders & Grevesse 1989), while the center energy of the 6.4 keV line and its flux were free parameters. We simultaneously fit this model to the FIs and BI spectra, and found a line-like residual at 7.0–7.1 keV, with the flux of ~ 10 –20% of the 6.4 keV (Fe I K α) line. From the energy and flux, the residual is likely to be the K β of neutral Fe. We then added second narrow Gaussian for the Fe I K β line, fixing its center energy to 1.103 times of that of K α . This model was accepted as is shown in figure 5, while the best-fit parameters are listed in table 2.

Table 2. The best-fit parameters of the spectral fittings to the background (GCDX) subtracted spectra of M 359.43–0.07 and M 359.47–0.15.

Parameter	M 359.43–0.07	M 359.47–0.15
Absorbed power-law model:		
Column density N_{H} (10^{23}cm^{-2})	0.92(0.48 – 1.41)	0.82(0.65 – 1.18)
Photon index	1.67(1.51 – 1.82)	1.61(1.52 – 1.86)
Gaussian 1 (FeI $K\alpha$):		
Line energy (keV)	6.41(6.39 – 6.42)	6.41(6.40 – 6.42)
Line flux ($10^{-6}\text{ph cm}^{-2}\text{s}^{-1}$) *	6.43(5.27 – 7.39)	8.82(7.87 – 10.0)
Equivalent width (keV)	2.18(1.79 – 2.51)	1.96(1.75 – 2.23)
Gaussian 2 (FeI $K\beta$):		
Line energy (keV) [†]	7.07	7.07
Line flux ($10^{-6}\text{ph cm}^{-2}\text{s}^{-1}$) *	1.05(0.43 – 2.14)	1.91(1.22 – 3.00)
Flux ($10^{-13}\text{erg cm}^{-2}\text{s}^{-1}$) [‡]	2.70	4.11
$\chi^2/\text{d.o.f.}$	27.92/41	49.67/46

90% confidence limits are in parentheses.

* Line fluxes are not corrected for the absorption.

[†] The line center is fixed so that the energy ratio is 1.103 ($K\beta/K\alpha=7.058\text{keV}/6.400\text{keV}$).

[‡] Observed flux of the diffuse emission in the energy band of 3 – 10 keV. Absorption is not corrected.

4. Discussion

We detected four 6.4 keV clumps, M 359.43–0.07, M 359.47–0.15, M 359.43–0.12, and M 359.38–0.00 with Suzaku. From the former bright clumps, M 359.43–0.07 and M 359.47–0.15, we found $K\alpha$ and $K\beta$ -lines from FeI. The most important fact is that EWs of the $K\alpha$ -lines are extremely large as ~ 2 keV (section 3.3). These large EWs are independently supported by the analysis of the GCDX in the Sgr C regions (section 3.2), and hence are highly reliable. We note that Yusef-Zadeh et al. (2007) reported small $EW_{6.4}$ from all the clumps, but their estimation was based on the spectra where no GCDX is subtracted.

4.1. Comparison with the Past X-Ray Observations

Murakami et al. (2001b) found excess emission at $(l, b) = (359^\circ 43, -0^\circ 04)$ in the X-ray image of the 5.8–7.0 keV band. Although the energy resolution was limited, an emission line at the energy consistent with FeI- $K\alpha$ line was found. Hence Murakami et al. (2001b) regarded this clump as an XRN.

The Suzaku source M 359.43–0.07 is located in the ASCA clump, but the peak position is systematically shifted. For comparison, we extracted the Suzaku spectrum from the same source and background regions as those of the ASCA clump (Murakami et al. 2001b). The background subtracted spectrum has the 6.4 keV line flux of $1.8_{-0.2}^{+0.3} \times 10^{-5}\text{ph cm}^{-2}\text{s}^{-1}$ (ab-

sorption uncorrected), which agrees with that of the ASCA clump ($3.5_{-2.2}^{+1.4} \times 10^{-5}$ ph cm $^{-2}$ s $^{-1}$). With Suzaku, we found that the surface brightness ratio of the 6.4 keV emission lines between the M 359.43–0.07, the ASCA clump and the outer background region are approximately 3:2:1 (1.9, 1.4, and 0.6 in the unit of 10^{-6} ph cm $^{-2}$ s $^{-1}$ arcmin $^{-2}$). Hence no significant detection of the full region of the ASCA clump in figure 2(b) may be due to its relatively lower surface brightness than M 359.43–0.07. On the other hand, no ASCA detection of M 359.43–0.07 is puzzling, although possible time variability can not be excluded. ASCA also detected no flux from the other bright Suzaku source M 359.47–0.15. However, this source is near the edge of the ASCA field.

The Suzaku spectrum of the whole Sgr C region (figure 1) shows the EWs of 458_{-10}^{+12} eV and 420_{-19}^{+10} eV for the 6.4 keV and 6.7 keV emission lines, respectively. The surface brightness in the 5–8 keV energy band is 7.1×10^{-14} erg cm $^{-2}$ s $^{-1}$ arcmin $^{-2}$. The Chandra analysis of the same region, in which point sources cataloged in the list of Munro et al. (2006) are excluded, shows that the EWs of the 6.4 keV and 6.7 keV emission lines are 460 ± 100 eV and ~ 400 eV, respectively. The surface brightness in the 5–8 keV band is $\sim 7.5 \times 10^{-14}$ erg cm $^{-2}$ s $^{-1}$ arcmin $^{-2}$ (figure 1b in Yusef-Zadeh et al. 2007). These are very similar to those of Suzaku, and hence point source contribution with the flux level larger than 1×10^{-13} erg cm $^{-2}$ s $^{-1}$ (Munro et al. 2006) may not be large, at least in the whole Sgr C region.

Detailed comparison in the smaller scale emission, however, shows significant differences. M 359.47–0.15 and a part of M 359.43–0.07 can be seen in the narrow band image at 6.4 keV with Chandra (figure 5a in Yusef-Zadeh et al. 2007). However, M 359.43–0.07 is not found in the EW map of Chandra (figure 5c in Yusef-Zadeh et al. 2007). This is a puzzle, because the Suzaku EW of M 359.43–0.07 is one of the largest among cited regions in the NXB-subtracted spectra. One possibility is a time variability as was found in Sgr B2 and Radio Arc regions (Munro et al. 2007; Koyama et al. 2008a; Inui et al. 2008). In the Chandra image of the 2–6 keV band (figure 1a of Yusef-Zadeh et al. 2007), a clump named as G 359.45–0.07 is found. However Suzaku found no excess in this region with the 6.4 keV line, and hence G 359.45–0.07 would not be 6.4 keV line emitter. Conversely no excess from M 359.38–0.00 is found with either Chandra or ASCA, possibly due to limited flux, and hence this is a new 6.4 keV clump found with the Suzaku satellite.

4.2. Ionization Mechanism

Two scenarios have been proposed for the origin of the 6.4 keV emission line from MCs in the GC region. One is X-ray photo ionization by external X-ray sources (the XRN scenario) (Koyama et al. 1996; Sunyaev & Churazov 1998; Park et al. 2004). The other is the inner shell ionization by the impact of LECRe (the electron bombardment scenario) (Valinia et al. 2000; Yusef-Zadeh et al. 2002). The LECRe scenario expects $EW_{6.4}$ of ~ 300 eV for the solar abundance Fe (Tatischeff 2003; Yusef-Zadeh et al. 2007), and hence is difficult to explain the

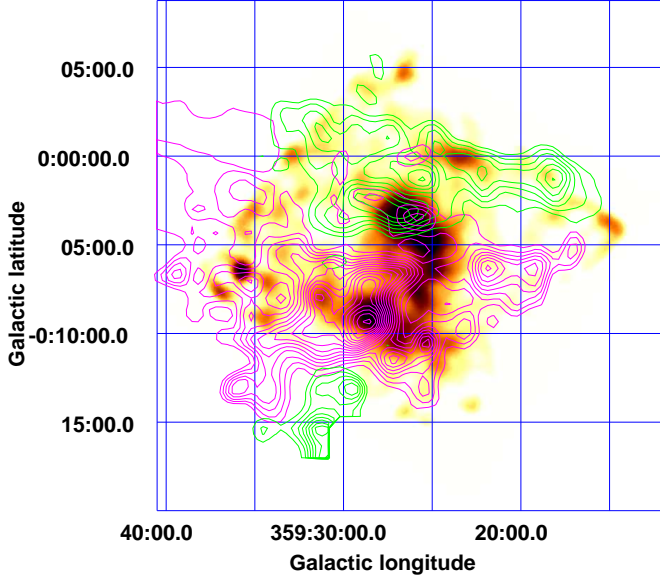


Fig. 6. The contours of channel map of CS $J = 1 - 0$ emission line overlaid on the narrow band image at 6.4 keV shown in figure 2(b). The first contour level and contour interval are 14.3 and 4.8 K km s⁻¹, respectively. Emission in the velocity ranges of -130 to -90 km s⁻¹ is shown with green and that of -80 to -30 km s⁻¹ is magenta, respectively.

observed large $EW_{6.4}$ of ~ 2 keV, unless Fe is extremely over-abundant by a factor of 6–7. We found no observational evidence for such over-abundance. On the other hand, XRN scenario naturally explain the large $EW_{6.4}$ of the M 359.43–0.07 and M 359.47–0.15, and hence is more likely.

4.3. Photo-Ionization Source

Since the typical absorption toward GC is $\sim 0.6 \times 10^{23}$ H cm⁻² (Rieke et al. 1989; Sakano et al. 2002), intrinsic absorption depth of M 359.43–0.07 and M 359.47–0.15 are $\lesssim 0.8 \times 10^{23}$ H cm⁻² and $\lesssim 0.6 \times 10^{23}$ H cm⁻², respectively. The areas of M 359.43–0.07 and M 359.47–0.15 shown in figure 2(b) are 7 arcmin², then their masses are estimated to be $\lesssim 4 \times 10^4$, $\lesssim 3 \times 10^4$ solar mass, respectively. From these masses and fluxes of the 6.4 keV lines, the luminosity of photo-ionizing source can be estimated following Sunyaev & Churazov (1998) as $\gtrsim 1 \times 10^{38}$ erg s⁻¹ and $\gtrsim 2 \times 10^{38}$ erg s⁻¹.

There is no X-ray object bright enough inside or nearby Sgr C region. Even the brightest near-by sources, KS 1741–293 and the Great Annihilator (1E 1740.7–2943) are impossible to explain this luminosity. Thus we arrive to the same conclusion for the 6.4 keV clumps origin near Sgr B2, a past Sgr A* activity of $\gtrsim 1 \times 10^{38}$ erg s⁻¹ at 240 yr ago.

4.4. Comparison with the Molecular Line Observations

The absorption column derived from the background-subtracted spectra of M 359.43–0.07 and M 359.47–0.15 are $N_{\text{H}} \sim 1 \times 10^{23} \text{ H cm}^{-2}$. We require similar amounts of column in the MCs that corresponds to M 359.38–0.00 and M 359.43–0.12. Referring the CS molecular line map over the velocity range of $V_{\text{LSR}} = -200$ to $+200 \text{ km s}^{-1}$ (Tsuboi et al. 1999, and the electric data), we searched for possible counterpart of the 6.4 keV clumps with $N_{\text{H}} \geq 10^{23} \text{ H cm}^{-2}$ (figure 6).

M 359.43–0.07 : MCs of $N_{\text{H}} \sim 10^{23} \text{ H cm}^{-2}$ are seen both in the velocity ranges of -50 to -70 km s^{-1} (also Yusef-Zadeh et al. 2007) and -90 to -110 km s^{-1} (also Murakami et al. 2001b).

M 359.47–0.15 : An MC with $N_{\text{H}} \geq 10^{23} \text{ H cm}^{-2}$ in the velocity range of -50 to -70 km s^{-1} exists in this region. M 359.47–0.15 is located in the western edge of -65 km s^{-1} MC as is also noticed by Yusef-Zadeh et al. (2007). There is no other MC of $\sim 10^{23} \text{ H cm}^{-2}$ in the other velocity range.

M 359.38–0.00 : No MC is seen in the -50 to -70 km s^{-1} band but an MC in the velocity range of -110 to -130 km s^{-1} is associated to the 6.4-keV clump; The column density of this radio cloud is roughly half of those in the directions of M 359.43–0.07 and M 359.47–0.15.

M 359.43–0.12 : There is a weaker peak in the -130 to -120 km s^{-1} band than that at M 359.38–0.00.

Sofue (1995) and Sawada et al. (2004) proposed that molecular gases in the GC region consists of two arms, Arm I and Arm II. The -130 to -90 km s^{-1} MC is physically associated with Arm I, while the -80 to -30 km s^{-1} MC is a part of Arm II. M 359.38–0.00 and M 359.47–0.15 belong to Arm I and Arm II, respectively, while M 359.43–0.07 has both possibilities. Since Arm II is located far side of Arm I (Sofue 1995; Sawada et al. 2004), X-rays from Sgr A* of several hundred years ago arrived at M 359.47–0.15 probably earlier than M 359.38–0.00.

5. Summary

1. We found four diffuse 6.4 keV clumps, M 359.43–0.07, M 359.47–0.15, M 359.43–0.12 and M 359.38–0.00 in the Sgr C region. The last one, M 359.38–0.00 is newly discovered.
2. The spectra of the two bright clumps, M 359.43–0.07 and M 359.47–0.15, have power-law of photon index of 1.6–1.7 with a very large $EW_{6.4}$ of 2.0–2.2 keV, the largest $EW_{6.4}$ among the 6.4 keV clumps in the GC.
3. The large $EW_{6.4}$ supports that the origin of 6.4 keV clumps is due to X-ray reflection irradiated by hard X-ray sources.
4. M 359.38–0.00 and M 359.47–0.15 possibly associate with MCs in different velocity ranges, indicating these are located in the different molecular arms.

We are grateful to all the members of the Suzaku hardware and software teams, and the science working group. This work was supported by the Grant-in-Aid for the Global COE Program “The Next Generation of Physics, Spun from Universality and Emergence” from the Ministry of Education, Culture, Sports, Science and Technology (MEXT) of Japan. HN and YH are financially supported by the Japan Society for the Promotion of Science.

References

- Anders, E., & Grevesse, N. 1989, *Geochim. Cosmochim. Acta*, 53, 197
- Balucinska-Church, M., & McCammon, D. 1992, *ApJ*, 400, 699
- Baganoff, F. K., et al. 2001, *Nature*, 413, 45
- Baganoff, F. K., et al. 2003, *ApJ*, 591, 891
- Inui, T., Koyama, K., Matsumoto, H., & Tsuru, T. G. 2008, *PASJ*, accepted
- Koyama, K., Awaki, H., Kunieda, H., Takano, S., Tawara, Y. Yamauchi, S., Hatsukade, I., & Nagase, F. 1989, *Nature*, 339, 603
- Koyama, K., Maeda, Y., Sonobe, T., Takeshima, T., Tanaka, Y., & Yamauchi, S. 1996, *PASJ*, 48, 249
- Koyama, K., et al. 2007a, *PASJ*, 59, S23
- Koyama, K., et al. 2007b, *PASJ*, 59, S245
- Koyama, K., et al. 2008a, *PASJ*, 60, S201
- Koyama, K., et al. 2008b, *PASJ*, accepted
- Liszt, H. S., & Spiker, R. W. 1995, *ApJS*, 98, 259
- Markevitch, M., Sunyaev, R. A., & Pavlinsky, M. 1993, *Nature*, 364, 40
- Mitsuda, K., et al. 2007, *PASJ*, 59, S1
- Muno, M. P., Bauer, F. E., Bandyopadhyay, R. M., & Wang, Q. D. 2006, *ApJS*, 165, 173
- Muno, M. P., Baganoff, F. K., Brandt, W. N., Park, S., & Morris, M. R. 2007, *ApJL*, 656, L69
- Murakami, H., Koyama, K., & Maeda, Y. 2001a, *ApJ*, 558, 687
- Murakami, H., Koyama, K., Tsujimoto, M., Maeda, Y., & Sakano, M. 2001b, *ApJ*, 550, 297
- Nobukawa, M., et al. 2008, *PASJ*, 60, S191
- Park, S., Muno, M. P., Baganoff, F. K., Maeda, Y., Morris, M., Howard, C., Bautz, M. W., & Garmire, G. P. 2004, *ApJ*, 603, 548
- Predehl, P., Costantini, E., Hasinger, G., & Tanaka, Y. 2003, *Astronomische Nachrichten*, 324, 73
- Revnivtsev, M. G., et al. 2004, *A&A*, 425, L49
- Rieke, G. H., Rieke, M. J., & Paul, A. E. 1989, *ApJ*, 336, 752
- Sakano, M., Koyama, K., Murakami, H., Maeda, Y., & Yamauchi, S. 2002, *ApJS*, 138, 19
- Sawada, T., Hasegawa, T., Handa, T., & Cohen, R. J. 2004, *MNRAS*, 349, 1167
- Serlemitsos, P. J., et al. 2007, *PASJ*, 59, S9
- Sofue, Y. 1995, *PASJ*, 47, 527
- Sunyaev, R. A., Markevitch, M., & Pavlinsky, M. 1993, *ApJ*, 407, 606
- Sunyaev, R., & Churazov, E. 1998, *MNRAS*, 297, 1279
- Tatischeff, V. 2003, *EAS Publications Series*, 7, 79, (astro-ph/0208397v1)
- Tawa, N., et al. 2008, *PASJ*, 60, S11

- Tsuboi, M., Handa, T., & Ukita, N. 1999, ApJS, 120, 1
- Uchiyama, Y., et al. 2008, PASJ, 60, S35
- Valinia, A., Tatischeff, V., Arnaud, K., Ebisawa, K., & Ramaty, R. 2000, ApJ, 543, 733
- Yamauchi, S., Kawada, M., Koyama, K., Kunieda, H., Tawara, Y., & Hatsukade, I. 1990, ApJ, 365, 532
- Yusef-Zadeh, F., Law, C., & Wardle, M. 2002, ApJL, 568, L121
- Yusef-Zadeh, F., Muno, M., Wardle, M., & Lis, D. C. 2007, ApJ, 656, 847